Electronic Supplementary Information

Insight into the photoelectric characteristic and photocatalytic water splitting in van der Waals heterostructures Cs_2PbI_4/MX_2 (M=Mo, W; X=Se, S)

Wei-Bing Zhang,[1,2] Ai-Jie Mao[2,*], Hua-Yun Geng [3], Xiang-Rong Chen[2,*]

[1]School of Big Data and Artifcial Intelligence, Chengdu Technological University, Chengdu 611730, China;

[2] College of Physics, Sichuan University, Chengdu 610064, China;

[3] National Key Laboratory for Shock Wave and Detonation Physics Research, Institute of Fluid Physics, CAEP, Mianyang 621900, China

Abstract

The photoelectric characteristic and photocatalytic water splitting in van der Waals heterostructures Cs_2PbI_4/MX_2 (M=Mo,W; X=Se, S) were carried out based on first principle calculations. Four stable heterostructures were obtained with indirect narrow gaps. Among them, $Cs_2PbI_4/MoSe_2$, Cs_2PbI_4/MoS_2 and Cs_2PbI_4/WSe_2 belong to type-II heterostructures, and Cs_2PbI_4/WS_2 is type-I heterostructure. High optical absorption efficiency and high carrier mobility imply that type-I heterostructure Cs_2PbI_4/WS_2 has a broad potential application prospect in light-emitting devices. Moreover, the optical absorption efficiency up to $10^{-5}cm^{-1}$, the spatial separation interval of photogenerated electron-hole (~3.30), and type-II band edge alignment

* *Corresponding authors. E-mail*: scu_mij@126.com; xrchen@scu.edu.cn

mean that heterostructures are easy to realize electron-hole separation and transfer, reduce the recombination probability of electron and holes, and thus enabling solar energy conversion and highly efficient photocatalytic water splitting. Especially, $Cs_2PbI_4/MoSe_2$ heterostructure can trigger HER and OER reaction spontaneously at *pH*=0 under equilibrium potential 1.23 V with a limiting reaction barrier of 1.16 eV for OER, which is close to 1.128 eV in $WSe_2/MoSe_2$ heterojunction reported recently, implying that its may be an excellent photocatalyst. In addition, the limiting reaction barrier of Cs_2PbI_4/WSe_2 heterostructure is 1.27 V, low overpotential for OER is 0.31 V, and high power conversion efficiency indicating that it may have a potential applications in both solar cells and photocatalytic water splitting.

Computational details The Heyd-Scuseria-Ernzerhof (HSE06) hybrid functional included the SOC effect is employed in simulating the electric properties of heterostructures.[1] The cutoff energy was set to 350 eV, and the Convergence criteria for energy and force are set at 10^{-5} eV and 0.002 eV/Å, respectively. The Brillouin zone grid is set to 6×4×1 for $1\times\sqrt{2}\,Cs_2PbI_4/2\times\sqrt{7}\,WSe_2$, $1\times\sqrt{2}\,Cs_2PbI_4/2\times\sqrt{7}\,WSe_2$, and $1\times\sqrt{2}\,Cs_2PbI_4/2\times\sqrt{7}\,WSe_2$ heterostructures, respectively.

The Gibbs free energies for the hydrogen evolution reaction (HER) and oxygen evolution reaction (OER) and are estimated by means of the model proposed by Nørskov et al.[2-3]

The HER can be driven along the following steps:

$$* + H^+ + e^- \rightarrow * H \quad (1)$$

$$* H + H^+ + e^- \rightarrow * + H_2 \quad (2)$$

The corresponding free energy $\Delta G_{*\mathrm{H}}$ is obtained by the following formula:

$$\Delta G_{*\mathrm{H}} = \Delta E_{*\mathrm{H}} + \Delta E_{\mathrm{ZPE}} - T\Delta S \quad (3)$$

$$\Delta E_{*\mathrm{H}} = E_{*\mathrm{H}} - E* - 1/2\, E_{\mathrm{H2}} \quad (4)$$

where ΔE_{*H} is the hydrogen chemisorption energy , where E_{*H}, $E*$ and E_{H2} are the energies of absorbed slab, pure slab and H_2 gas, respectively.

Moreover, the OER follows four elementary steps:

$$* + H_2O \rightarrow OH + H^+ + e^- \quad (5)$$

$$* OH \rightarrow * O + H^+ + e^- \quad (6)$$

$$* O + H_2O \rightarrow * OOH + H^+ + e^- \quad (7)$$

$$* OOH \rightarrow * + O_2 + H^+ + e^- \quad (8)$$

wherein, $*$ represents the absorption site on the slab for intermediates.

The Gibbs reaction free energy (ΔG) of each step is estimated by the following formula:

$$\Delta G = \Delta E + \Delta E_{\mathrm{ZPE}} - T\Delta S + \Delta G_U + \Delta G_{\mathrm{pH}} \quad (9)$$

where, ΔE is the total energy difference between reactants and products of reactions, ΔE_{ZPE} is the zero point energy correction, ΔS is the vibrational entropy change at finite temperature T, $\Delta G_U = -eU$ incorporates the effect of the electrode potential, where e is elementary charge, U is the electrode potential (U=1.23), ΔG_{pH} is the correction of the H^+ free energy. pH = 0 are employed in our calculations.

Table S1. The lattice parameters *a* and *b* of the optimized monolayers Cs_2PbI_4 and MX_2 with different size. And the lattice parameters *a*, and *b* of the constructed initial heterostructures Cs_2PbI_4/MX_2 (M=Mo,W;X=Se,S).

Heterostructures	Configurations	Cs_2PbI_4		MX_2		initial heterostructures	
		a(Å)	*b*(Å)	*a*(Å)	*b*(Å)	*a*(Å)	*b*(Å)
$Cs_2PbI_4/MoSe_2$	$1\times\sqrt{2}/2\times\sqrt{7}$	6.299	8.908	6.588	8.715	6.443	8.811
	$1\times\sqrt{5}/2\times4$	6.299	14.084	6.588	13.176	6.443	13.630
	$1\times1/2\times\sqrt{3}$	6.299	6.299	6.588	5.705	6.443	6.002
Cs_2PbI_4/WSe_2	$1\times\sqrt{2}/2\times\sqrt{7}$	6.299	8.908	6.580	8.704	6.439	8.806
	$1\times\sqrt{5}/2\times4$	6.299	14.084	6.580	13.160	6.439	13.622
Cs_2PbI_4/MoS_2	$1\times\sqrt{2}/2\times\sqrt{7}$	6.299	8.908	6.328	8.372	6.314	8.640
	$\sqrt{2}\times2/3\times\sqrt{13}$	8.907	12.598	9.492	11.408	9.200	12.002
Cs_2PbI_4/WS_2	$1\times\sqrt{2}/2\times\sqrt{7}$	6.299	8.908	6.365	8.419	6.332	8.664

Table S2. The band gap *E*(*eV*), electron affinity *A*(eV), and ionization energy *I*(eV) of monolayers Cs_2PbI_4 and MX_2 based on HSE+SOC and PBE functional, respectively.

	Cs_2PbI_4	$MoSe_2$	WSe_2	MoS_2	WS_2
E(PBE)	1.83	1.51	1.64	1.74	1.87
-*A*(PBE)	-3.130	-3.758	-3.428	-4.169	-3.804
-*I* (PBE)	-4.961	-5.267	-5.074	-5.905	-5.679
E($HSE^{\alpha=0.25}$+SOC)	1.62	2.44	2.11	2.42	2.47
E(HSE^{α}+SOC)	$1.89^{\alpha=0.35}$	$1.56^{\alpha=0.07}$	$1.67^{\alpha=0.15}$	$1.87^{\alpha=0.10}$	$2.01^{\alpha=0.15}$
-*A*(HSE^{α}+SOC)	-3.521	-3.995	-3.591	-4.369	-3.904
-*I*(HSE^{α}+SOC)	-5.406	-5.555	-5.262	-6.237	-5.920
Experiment[4]	1.86	1.57	1.65	1.90	1.94-1.99

Table S3. The band gap (eV),VBM edge (eV) and CBM edge (eV) of monolayers Cs_2PbI_4 and MX_2 in heterostructures based on HSE+SOC and PBE functional, respectively.

	Functional	Cs_2PbI_4	$MoSe_2$	Cs_2PbI_4	WSe_2	Cs_2PbI_4	MoS_2	Cs_2PbI_4	WS_2
Bandgap		2.065	1.488	1.892	1.733	2.031	1.231	1.431	2.054
CBM	PBE	1.857	1.197	1.686	1.244	2.019	0.940	1.266	1.283
VBM		-0.208	-0.290	-0.206	-0.489	-0.011	-0.291	-0.206	-0.269
Bandgap				1.773	1.867	1.631	1.519	1.622	1.824
CBM	HSE+SOC			1.552	1.464	1.412	1.191	1.397	1.535
VBM				-0.220	-0.403	-0.218	-0.329	-0.225	-0.289

Table S4. The open-circuit voltage (V_{OC}), conduction band offset (CBO) and power conversion efficiency (PCE) of Cs_2PbI_4/MSe_2 (M=Mo,W) heterostructures. E_d^g is donor bandgap based on PBE and HSE+SOC, respectively.

Functional	Heterostructure	Size	E_d^g	CBO	V_{oc}	PEC（%）
PBE	$Cs_2PbI_4/MoSe_2$	$1\times\sqrt{5}/2\times4$	2.065	0.660	1.405	17.1%
	Cs_2PbI_4/WSe_2	$1\times\sqrt{2}/2\times\sqrt{7}$	1.892	0.442	1.450	21.9%
HSE+SOC	$Cs_2PbI_4/MoSe_2$*	$1\times\sqrt{2}/2\times\sqrt{7}$	1.885	0.474	1.111	16.8%
	Cs_2PbI_4/WSe_2	$1\times\sqrt{2}/2\times\sqrt{7}$	1.773	0.088	1.385	23.9%

* represents the data based isolated monolayers.

Table S5. Carrier effective masses m_e and m_h, reduced mass μ, static dielectric constant ε and exciton binding energies of Cs_2PbI_4/MSe_2 (M=Mo,W) heterostructures. Edg is donor bandgap based on PBE functional.

Heterostructure	Direction	m_e	m_h	μ	ε	E_e
$Cs_2PbI_4/MoSe_2$	*a*	0.266	2.26	0.238	5.233	0.473
	b	0.657	0.739	0.348	5.209	0.698
Cs_2PbI_4/WSe_2	*a*	0.598	6.419	0.547	4.905	1.237
	b	1.645	0.196	0.175	5.014	0.379
Cs_2PbI_4/MoS_2	*a*	0.476	0.591	0.264	5.035	0.567
	b	0.471	0.958	0.316	5.107	0.659
Cs_2PbI_4/WS_2	*a*	0.854	0.694	0.383	4.758	0.920
	b	0.089	0.733	0.794	4.787	1.885

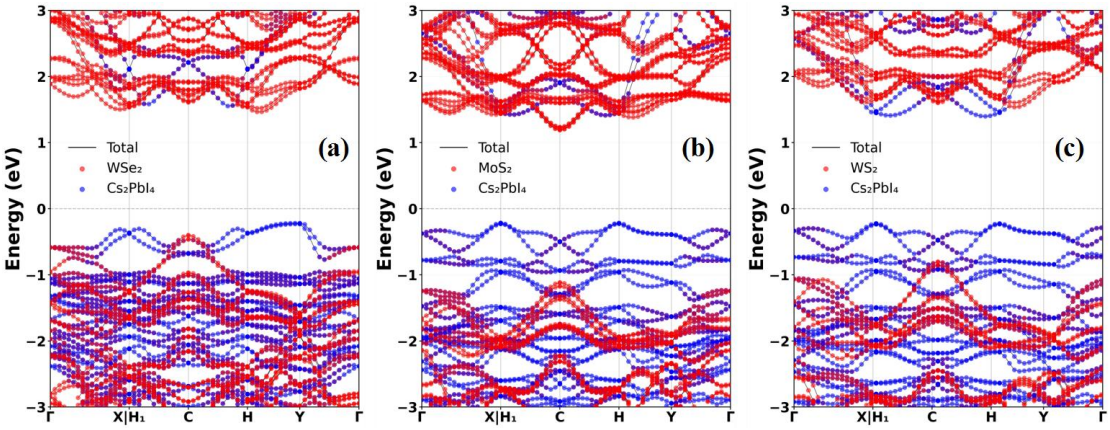

Fig.S1. Projected band structures of heterostructures (a) Cs_2PbI_4/WSe_2, (b)Cs_2PbI_4/MoS_2 and (c)Cs_2PbI_4/WS_2 based on HSE+SOC.

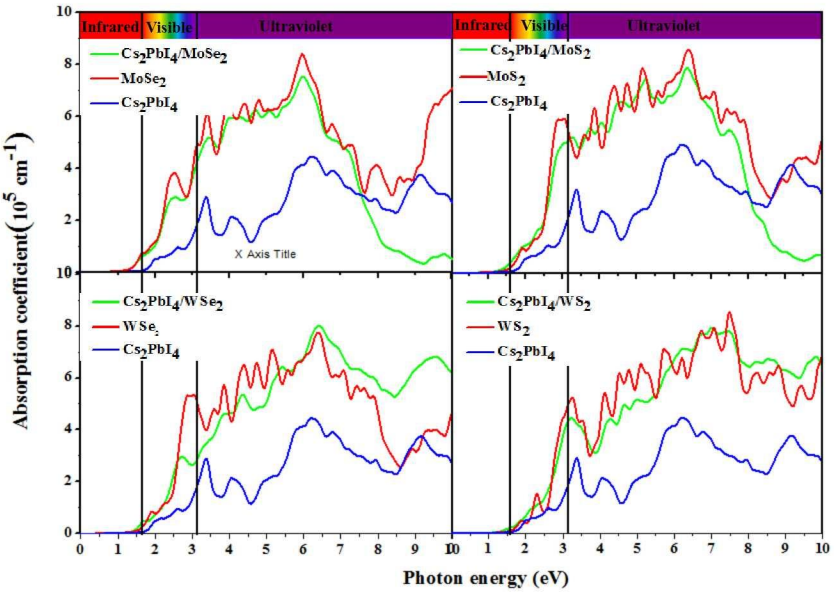

Fig. S2. Optical absorption of monolayer Cs_2PbI_4, MX_2 (M=Mo,W;X=Se,S) and four stable heterostructures $Cs_2PbI_4/MoSe_2$, $Cs2PbI_4/WSe_2$, Cs_2PbI_4/MoS_2 and Cs_2PbI_4/WS_2.

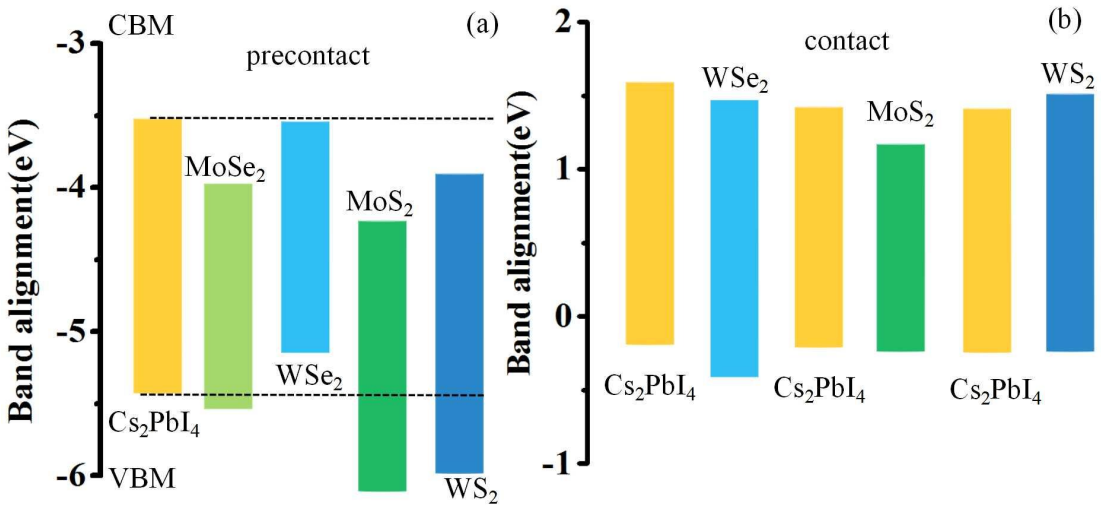

Fig. S3. Band alignments of monolayers Cs_2PbI_4, WSe_2, MoS_2, and MoS_2 in precontact state (a) and contact state (b) based on HSE+SOC functional.

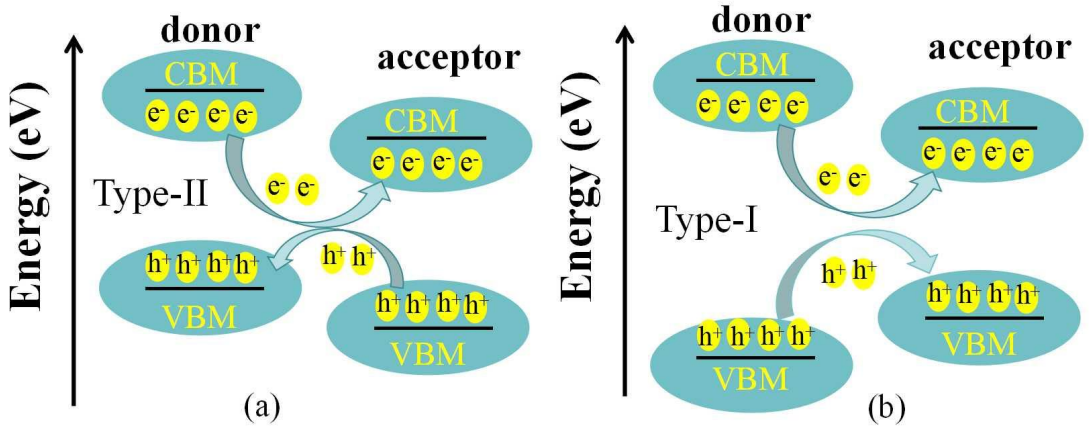

Fig. S4. The mechanism for electron-hole pair separation in heterostructures, (a) Type-II, (b) Type-I.

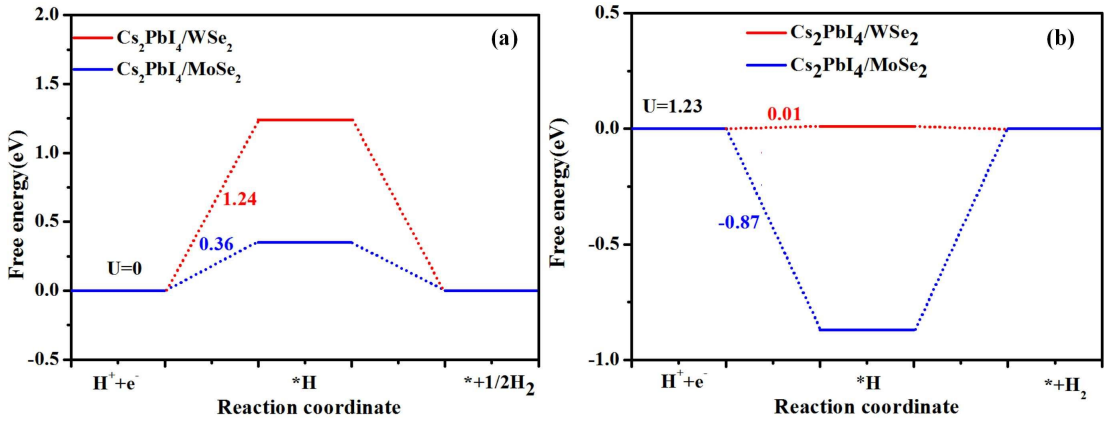

Fig. S5. Gibbs free energy diagram for HER at *pH*=0 under zero cell potential U=0 and equilibrium potential U=1.23V.

References

1) J. Heyd and G. E. Scuseria, J. Chem. Phys., 2004, 120, 7274– 7280.

2) J. K. Nørskov, J. Rossmeisl, A. Logadottir, L. Lindqvist, J. R. Kitchin, T. Bligaard and H. Jonsson, J. Phys. Chem. B., 2004, 108, 17886–17892.

3) J. K. Nørskov, T. Bligaard, A. Logadottir, J. Kitchin, J. G. Chen, S. Pandelov and U. Stimming, J. Electrochem Soc, 2005, 152, J23.

4) C. H. Chang, X. F. Fan,S. H. Lin, J. L. Kuo, *Phys. Rev. B*. 2013, 88, 195420.